Available online at www.sciencedirect.com

ScienceDirect

Nuclear Physics A 947 (2016) 161–172

NUCLEAR PHYSICS A

www.elsevier.com/locate/nuclphysa

Elastic and inelastic scattering of ^{15}N ions by ^{9}Be at 84 MeV

A.T. Rudchik [a,*], K.A. Chercas [a], K.W. Kemper [b], K. Rusek [c], A.A. Rudchik [a], O.V. Herashchenko [a], E.I. Koshchy [d], Val.M. Pirnak [a], E. Piasecki [c], A. Trzcińska [c], S.B. Sakuta [e], R. Siudak [f], I. Strojek [g], A. Stolarz [c], A.P. Ilyin [a], O.A. Ponkratenko [a], Yu.M. Stepanenko [a], Yu.O. Shyrma [a], A. Szczurek [f], V.V. Uleshchenko [a]

[a] *Institute for Nuclear Research, Ukrainian Academy of Sciences, Prospect Nauki 47, 03680 Kyiv, Ukraine*
[b] *Physics Department, Florida State University, Tallahassee, FL 32306-4350, USA*
[c] *Heavy Ion Laboratory of Warsaw University, ul. L. Pasteura 5A, PL-02-093 Warsaw, Poland*
[d] *Kharkiv National University, pl. Svobody 4, 61077 Kharkiv, Ukraine*
[e] *Russian Research Center "Kurchatov Institute", Kurchatov Sq. 1, 123182 Moscow, Russia*
[f] *H. Niewodniczański Institute of Nuclear Physics, Polish Academy of Sciences, ul. Radzikowskiego 152, PL-31-342 Cracow, Poland*
[g] *National Center for Nuclear Researches, ul. Hoża 69, PL-00-681 Warsaw, Poland*

Received 2 September 2015; received in revised form 24 December 2015; accepted 2 January 2016

Available online 6 January 2016

Abstract

Angular distributions of the ^{9}Be + ^{15}N elastic and inelastic scattering were measured at $E_{\rm lab}(^{15}{\rm N}) =$ 84 MeV ($E_{\rm c.m.} = 31.5$ MeV) for the 0–6.76 MeV states of ^{9}Be and 0–6.32 MeV states of ^{15}N. The data were analyzed within the optical model and coupled-reaction-channels method. The elastic and inelastic scattering, spin reorientations of ^{9}Be in ground and excited states and ^{15}N in excited states as well as the most important one- and two-step transfer reactions were included in the channels-coupling scheme. The parameters of the ^{9}Be + ^{15}N optical potential of Woods–Saxon form as well as deformation parameters of these nuclei were deduced. The analysis showed that the ^{9}Be + ^{15}N pure potential elastic scattering dominates at the forward angles whereas the ground state spin reorientation of ^{9}Be gives a major contribution to

* Corresponding author.
E-mail address: rudchik@kinr.kiev.ua (A.T. Rudchik).

http://dx.doi.org/10.1016/j.nuclphysa.2016.01.002

the elastic scattering cross sections at the large angles. Contributions from particle transfers are found to be negligible for the present scattering system.

Keywords: NUCLEAR REACTIONS ^{9}Be(^{15}N, ^{15}N), $E = 84$ MeV; measured particle spectra, $\sigma(\theta)$; deduced reaction mechanism features and Woods–Saxon potential parameters of the ^{9}Be + ^{15}N potential and deformation parameters of ^{9}Be and ^{15}N using coupled-reaction-channels analysis

1. Introduction

Early work to put heavy-ion elastic scattering potentials on a more fundamental level by the use of semi-microscopic double folding potentials [1] showed, that the majority of the interactions could be well described except for the three nuclei ^{6}Li, ^{7}Li and ^{9}Be. For these three nuclei, the strengths of the calculated real potentials had to be reduced by ∼0.6 [2,3]. Since these three nuclei have relatively low break up energies and strong polarizability, it was considered that these conditions produced the need for this strength reduction. In addition, ground state reorientation of the nuclei ^{7}Li and ^{9}Be could give contributions to the elastic scattering because of their large ground state quadrupole moments, further complicating our understanding of their scattering. Additional evidence for the possible anomalous nature of ^{6}Li and ^{7}Li elastic scattering was found, when analyzing powers were measured with polarized beams of Li isotopes [4]. The first rank analyzing powers (AP) were of opposite sign. If they arose from a spin–orbit interaction as was normally assumed they would have been of the same sign. Through coupled channels calculations with the M3Y interaction, it was shown that this difference in analyzing powers was due to virtual coupling to their excited states and continua. These results clearly indicated the influence of the internal structure of the projectile, and/or target on the elastic scattering, but this effect was only apparent through coupled channels calculations. The reason for not realizing the importance of the internal structure of the interacting nuclei earlier was that it was always possible to describe the data with different sets of optical model parameters.

Recently the role of projectile-target excitation in the elastic scattering of light heavy-ions has been revived as new detailed elastic scattering data has revealed anomalies in the extraction of Airy minima. For example, an analysis [5] of ^{16}O + ^{12}C elastic scattering data at the energy of $E_{\rm lab} = 281$ MeV showed a possible secondary bow [5] in nuclear rainbow scattering. This surprising result arose because of the existence of elastic scattering data at large angles ($\theta_{\rm c.m.} \approx 115°$) [6]. For a recent review of the history of rainbow scattering and its application to nuclear systems see Ohkubo and Hirabayashi [7]. The existence of this secondary nuclear rainbow was shown to be dynamically generated by the excitation of states in both the projectile and target through the use of coupled channels calculations [5]. This work and others prompted the examination of channel coupling in elastic scattering for the systems ^{16}O + ^{12}C [8] over a large projectile energy range as well as for the system ^{16}O + ^{14}C [9]. The fact that the ^{16}O + ^{12}C scattering is a strongly coupled system was found to be important for examining heavy-ion dynamic polarization potentials [10]. A slightly earlier analysis of high quality elastic and inelastic scattering data for the ^{16}O + ^{27}Al system demonstrated clearly the role played by inelastic target and projectile couplings in rainbow formation even for heavier systems [11]. These results demonstrated that the earlier observations of the influence of the projectile internal structure on the elastic scattering for light projectiles applies to the recently studied heavier systems. The neg-

ligible contribution of particle transfer channels in these analyses, as shown by previous analyses of the type carried out here [12], greatly simplifies our ability to isolate coupled channels effects.

To further explore the influence of the projectile-target internal structure on scattering, the systems ^{11}B + ^{14,15}N were measured and analyzed through coupled channels calculations. These systems showed considerable variation in the contributions to the scattering at large angles, with that for ^{11}B + ^{14}N [13], arising from a combination of potential and ground state reorientation effects with almost no contribution from transfer reactions. For ^{11}B + ^{15}N [14], the proton exchange contribution was needed in addition to the other contributions found for ^{11}B + ^{14}N, to fully explain the large angle scattering cross section. The forward angle scattering was produced by potential scattering for both systems with similar potential values.

In the present work, we study the elastic and inelastic scattering for the system ^{9}Be + ^{15}N. The large ground state quadrupole moment of ^{9}Be ($+4.9 \pm 0.3$ efm^2) makes this a perfect projectile to isolate the contribution of ground state reorientation to the large angle scattering cross section. In addition, the ground state ^{15}N spin of $1/2$ means there is no reorientation contribution to the scattering cross section and its excited states are only weakly populated in inelastic scattering. Previously, the reactions ^{9}Be(^{15}N, ^{14}O), (^{15}N, ^{17}F), (^{15}N, ^{12}N) were studied at 240 MeV [15–17] to determine the structure of the residual nuclei. However, no angular distribution data for the ^{9}Be(^{15}N, ^{15}N)^{9}Be elastic and inelastic scattering were reported and this is also true for elastic scattering at any energy, to the best of our knowledge. New data for the elastic and inelastic scattering of ^{15}N ions by ^{9}Be at 84 MeV are presented as are the results of an analysis within the coupled-reaction-channels (CRC) method. Considerable attention is given to exploring contributions from different particle transfer reactions since their presence can mask effects arising from inelastic scattering, especially at large angles.

The paper is organized as follows. Section 2 contains a brief summary of the experimental procedure, Section 3 gives the results of CRC calculations and the last section provides a summary of this work.

2. Experimental procedure

Angular distributions of the ^{9}Be + ^{15}N elastic and inelastic scattering were measured simultaneously with the ^{9}Be(^{15}N, X) transfer reactions, using the 84 MeV beam of ^{15}N from the cyclotron U-200P of the Heavy Ion Laboratory (HIL) of Warsaw University. The beam energy spread on the self-supporting 600 μg/cm^2 target foil of ^{9}Be did not exceed 0.5% FWHM. The experimental set-up ICARE [18] was used to perform the measurements.

The reaction products were detected by four ΔE–E-telescopes, each with a 40 μm silicon ΔE-detector and a 0.3 mm silicon E-detector. A typical $\Delta E(E)$-spectrum of the ^{9}Be(^{15}N, X) reaction products is presented in Fig. 1. As one can see, the reaction products with $Z = 3$–8 were well resolved by charge as well as mass.

Energy spectra of ^{9}Be and ^{15}N obtained at $\theta_{\rm lab} = 15^\circ$ are shown in Figs. 2(a) and 2(c). The curves show the contributions from multi-particle reactions. The residual energy spectra of ^{9}Be and ^{15}N obtained after subtraction of these backgrounds and peaks from the target admixtures are shown in Figs. 2(b) and 2(d) for the studied energy intervals. The curves show the symmetric Gauss functions fit to the spectra peaks. More information about the spectra procedures are given in our previous works [12].

The areas under the peaks of the residual ^{15}N and ^{9}Be spectra were used for the extraction of cross sections at the angles $\theta_{\rm c.m.}(^{15}{\rm N})$ and $\theta_{\rm c.m.}(^{15}{\rm N}) = 180^\circ - \theta_{\rm c.m.}(^{9}{\rm Be})$, respectively. In this

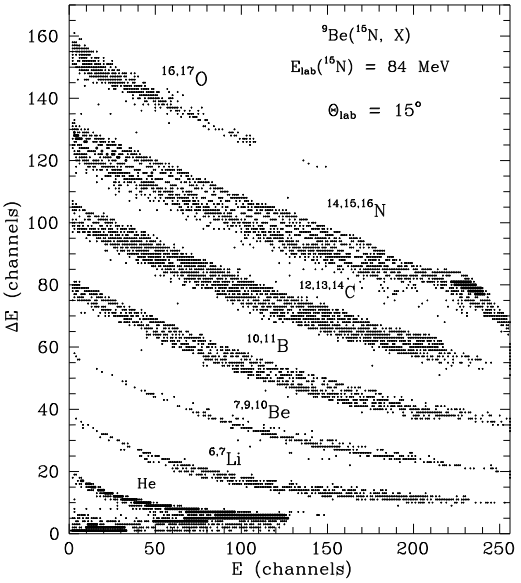

Fig. 1. Typical $\Delta E(E)$-spectrum of the ^{9}Be(^{15}N, X) reaction products at the energy $E_{\rm lab}(^{15}{\rm N}) = 84$ MeV.

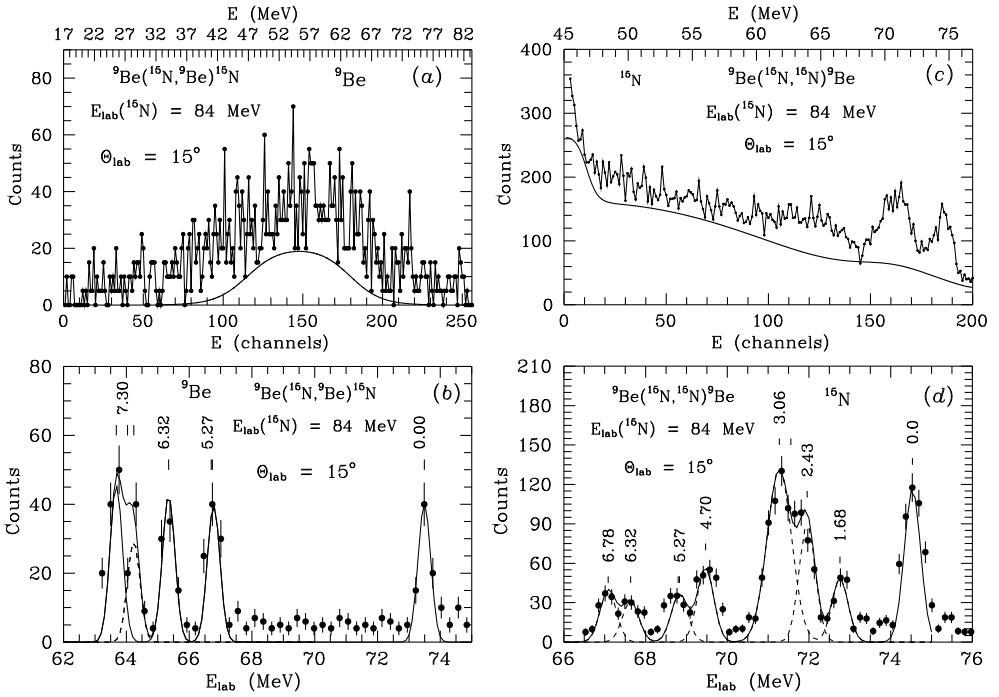

Fig. 2. Typical energy spectra of ^{9}Be from the ^{9}Be(^{15}N, ^{9}Be)^{15}N reaction (a) with multiparticle reaction backgrounds (curves show background forms), (b) after subtraction of the backgrounds (curves show the Gauss symmetric forms) and the ^{15}N spectra from the ^{9}Be(^{15}N, ^{15}N)^{9}Be reaction (c) with the backgrounds and (d) without the backgrounds (curves show the same as for the ^{9}Be spectra).

way, angular distributions for ^{9}Be(^{15}N, ^{15}N)^{9}Be scattering over the whole angular range were determined.

The total errors of the individual data points include the statistical errors of the extracted areas under the peaks and that of the background estimations and do not exceed 30–40%. The error bars on the data points show the error for each individual data point.

The angular distributions of the ^{9}Be + ^{15}N elastic scattering were normalized to the calculated optical model (OM) cross section at small angles where it is relatively independent of the nuclear potential parameters. The χ^2-criterion was used to obtain the normalization factor and an estimate of the absolute error is 20%. The same factor was used to normalize the angular distributions for both elastic and inelastic scattering data at the forward, middle and backward angles.

3. Data analysis

3.1. Calculation procedure

The data of ^{9}Be + ^{15}N elastic and inelastic scattering were analyzed by OM and CRC methods using optical model potentials in the entrance and exit channels of Woods–Saxon form

$$U(r) = -V_0\left[1+\exp\left(\frac{r-R_V}{a_V}\right)\right]^{-1} - iW_S\left[1+\exp\left(\frac{r-R_W}{a_W}\right)\right]^{-1} \tag{1}$$

and a Coulomb potential of a uniform charged sphere of radius R_C. Here

$$R_i = r_i(A_P^{1/3} + A_T^{1/3}),\ i = V, W, C, \tag{2}$$

where A_P, A_T are the mass numbers of ^{15}N and ^{9}Be. The parameter $r_C = 1.25$ fm was used in all calculations.

In the CRC analysis, the ^{9}Be + ^{15}N elastic and inelastic scattering for the transitions to the ground and excited states of ^{9}Be and ^{15}N, spin reorientation of ^{9}Be and most important transfer reactions were included in the channels coupling scheme. Fig. 3 shows the transitions to the excited states of ^{9}Be and ^{15}N. The arcs show the spin reorientations of ^{9}Be and ^{15}N in states with spins $I > 1/2$ (quadrupole transitions to the $I = 1/2$ states are forbidden). The diagrams of one- and two-step transfers included in the CRC calculations are presented in Fig. 4.

We assume that the rotations as well as vibrations of the ^{9}Be and ^{15}N nuclei are the dominant mechanisms for the low-energy excitations of these nuclei. The transitions to these rotational and vibrational states were calculated using the form-factors:

$$V_\lambda(r) = -\frac{\delta_\lambda}{\sqrt{4\pi}}\frac{dU(r)}{dr} \tag{3}$$

where δ_λ is the length of the λ-multipole deformation. The values of the deformation parameters δ_λ of ^{9}Be and ^{15}N obtained by fitting CRC-calculations to the ^{9}Be + ^{15}N inelastic scattering are listed in Table 1. Many parameters were found to be similar to those obtained from CRC-analyses of the inelastic scattering data of ^{11}B + ^{15}N [14], ^{9}Be + ^{12}C [19] and ^{9}Be + ^{11}B [20]. In Table 1 we list the parameters $\beta_\lambda^{a} = \delta_\lambda/R$ for the ^{9}Be + ^{15}N deformed potential ($R = 3.742$ fm) and β_λ^{b} for similar systems (Refs. [14,19,20]).

The spectroscopic amplitudes S_x of transfered clusters or nucleons x in the $A = C + x$ systems required for the CRC-calculations of the transfer reactions were obtained within the translational invariant shell model (TISM) [21] using the code DESNA [22,23] and tables of 1p-shell wave

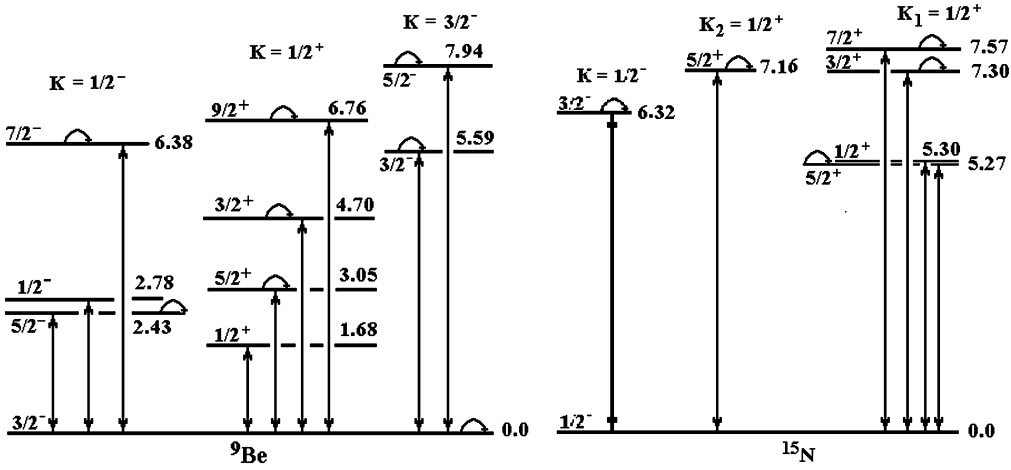

Fig. 3. Coupling schemes for the transitions to the excited states of ^{9}Be and ^{15}N. The arcs show the spin reorientations of ^{9}Be and ^{15}N in states with spins $I > 1/2$.

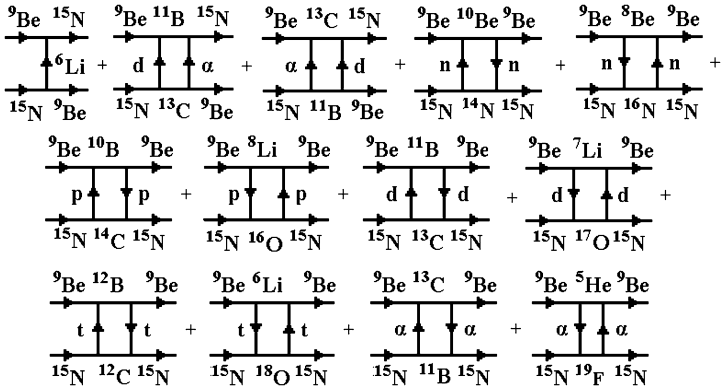

Fig. 4. Diagrams of one- and two-step transfers contributing to the ^{9}Be + ^{15}N scattering calculations.

functions from Ref. [24] calculated within the intermediate coupling shell-model [25]. The amplitudes S_x are listed in Table 2.

The wave function of the bound state of cluster x was calculated by fitting the energy eigenvalue to the x-cluster binding energy in the $A = C + x$ system by adjusting the depth of the Woods–Saxon potential with $a_V = 0.65$ fm and $r_V = 1.25A^{1/3}/(C^{1/3} + x^{1/3})$ fm.

The calculations of the ^{9}Be + ^{15}N elastic and inelastic scattering were performed with the following steps. The codes SPI-GENOA [26] and FRESCO [27] were used for the OM and CRC calculations, respectively. First, the ^{9}Be + ^{15}N double-folding potential was calculated with the code DFPOT [28,29] using the M3Y (Reid) nucleon–nucleon potential and charge distributions in ^{9}Be and ^{15}N [30]. The nuclear matter densities needed to calculate the ^{9}Be + ^{15}N double-folding potential were generated from the charge distributions by the method described in Refs. [28,29].

Then, the parameters of the real part of the ^{9}Be + ^{15}N potential of Woods–Saxon form (1) were fitted to the double-folded potential in the peripheral region ($R_V - a_V/2 < r < R_V +$

Table 1
Deformation parameters of ^{9}Be and ^{15}N.

Nucleus	E^* (MeV)	J^π	λ	δ_λ (fm)	β_λ [a]	System	β_λ [b]	Ref.
^{9}Be	0.000	$3/2^-$	2	2.4	0.641	^{9}Be + ^{12}C	0.667	[19]
	1.684	$1/2^+$	1	2.0	0.534		0.556	[19]
	2.429	$5/2^-$	2	2.4	0.641		0.667	[19]
			4	0.4	0.107		0.111	[19]
	2.780	$1/2^-$	2	2.4	0.641	^{9}Be + ^{11}B	0.687	[20]
	3.049	$5/2^+$	1	2.0	0.534		0.573	[20]
			3	1.0	0.267		0.286	[20]
	4.704	$3/2^+$	1	2.0	0.534		0.573	[20]
			3	1.0	0.267		0.286	[20]
	5.590	$3/2^-$	2	2.4	0.641	^{9}Be + ^{15}N		
	6.380	$7/2^-$	2	2.4	0.641			
			4	0.4	0.107			
	6.760	$9/2^+$	3	1.0	0.267			
			5	0.1	0.027			
^{15}N	5.270	$5/2^+$	3	1.0	0.267	^{11}B + ^{15}N	0.262	[14]
	5.299	$1/2^+$	1	1.0	0.267		0.262	[14]
	6.324	$3/2^-$	2	1.0	0.267		0.262	[14]
	7.155	$5/2^+$	3	1.0	0.267		0.262	[14]
	7.301	$3/2^+$	1	1.0	0.267		0.262	[14]
	7.567	$7/2^+$	3	1.0	0.267		0.262	[14]

[a] $\beta_\lambda = \delta_\lambda / R$ (for the ^{9}Be + ^{15}N deformed potential).
[b] β_λ from similar systems (Refs. [14,19,20]).

Table 2
Spectroscopic amplitudes for S_x of x-clusters in $A = C + x$ systems.

A	C	x	nL_j	S_x	A	C	x	nL_j	S_x
^{9}Be	^{5}He	α	$3S_0$	−0.810	^{13}C	^{9}Be	α	$2D_2$	0.504[a]
			$2D_2$	−0.536	^{15}N	^{9}Be	^{6}Li	$3S_1$	−0.274
^{9}Be	^{6}Li	t	$2P_{1/2}$	−0.192				$2D_1$	−0.069
			$2P_{3/2}$	−0.215[a]				$2D_2$	−0.207[a]
^{9}Be	^{7}Li	d	$2S_1$	−0.226[a]	^{15}N	^{11}B	α	$2D_2$	0.435[a]
			$1D_1$	0.111[a]	^{15}N	^{12}C	t	$2P_{1/2}$	0.380
			$1D_3$	−0.624[a]	^{15}N	^{13}C	d	$2S_1$	0.248[a]
^{9}Be	^{8}Li	p	$1P_{1/2}$	−0.375[a]				$1D_1$	0.444[a]
^{9}Be$^*_{5.59}$	^{8}Li	p	$1P_{1/2}$	−0.375[a]	^{15}N	^{14}C	p	$1P_{1/2}$	−0.598
^{9}Be	^{8}Be	n	$1P_{3/2}$	0.866	^{15}N	^{14}N	n	$1P_{1/2}$	−1.091[a]
^{10}Be	^{9}Be	n	$1P_{3/2}$	1.405[a]				$1P_{3/2}$	0.386
^{10}B	^{9}Be	p	$1P_{3/2}$	1.185	^{16}N	^{15}N	n	$1P_{3/2}$	−0.270
^{10}B	^{9}Be$^*_{5.59}$	p	$1P_{3/2}$	1.185	^{16}O	^{15}N	p	$1P_{1/2}$	−1.461[a]
^{11}B	^{9}Be	d	$2S_1$	0.607[a]	^{17}O	^{15}N	d	$2P_2$	−0.552
			$1D_1$	−0.109[a]	^{18}O	^{15}N	t	$2P_{1/2}$	−0.261[a]
			$1D_3$	0.610[a]	^{19}F	^{15}N	α	$3S_0$	−0.638
^{11}B	^{9}Be	t	$2P_{1/2}$	0.102[a]					
			$2P_{3/2}$	0.091					
			$1F_{5/2}$	0.512[a]					

[a] $S_{FRESCO} = (-1)^{J_C + j - J_A} S_x = -S_x$.

Table 3
Parameters of the ^{9}Be + ^{15}N potential.

V_0 (MeV)	r_V (fm)	a_V (fm)	W_S (MeV)	r_W (fm)	a_W (fm)	J_V/J_W (MeV fm^3)	R_V (fm)	R_W (fm)
170	0.793	0.800	12	1.250	0.800	367.3/81.7	4.08	5.31

$a_V/2$ fm). Next, the deduced parameters V_0, r_V, a_V for the real part of the potential (1) and initial parameters $r_W = 1.25$, $a_W = a_V$, $W = V_0/10$ for the imaginary part of this potential were used in the code SPI-GENOA to calculate the ^{9}Be + ^{15}N elastic scattering at small angles. Since the OM cross-sections at these small angles are relatively independent of the nuclear potential parameters, the measured data were normalized to these cross sections at small angles.

Next, the deduced normalization factor was used to normalize the measured ^{9}Be + ^{15}N elastic and inelastic scattering data over the full angular region. Then, the initial ^{9}Be + ^{15}N potential parameters were fitted to the normalized full angular range elastic scattering data with the code SPI-GENOA.

Finally, the deduced potential parameters $X_i = \{V_0, r_V, a_V, W_S, r_W, a_W\}$ from the OM analysis of the elastic scattering data were optimized in the CRC calculations with the channels-coupling scheme that included the elastic and inelastic scattering, spin reorientations of ^{9}Be in ground and excited states and ^{15}N in excited states as well as the most important one- and two-step transfer reactions. The ^{9}Be + ^{15}N potential parameters obtained in the CRC analysis of the data are listed in Table 3. In this table, the volume potential integrals per nucleon of J_V and J_W as well as mean-square-radii (MRS) R_V and R_W are also listed.

3.2. *Elastic scattering $^{9}Be + ^{15}N$*

The angular distribution of the measured ^{9}Be + ^{15}N elastic scattering are presented in Fig. 5(a) in cross-section units and in Fig. 5(b) in units of the Rutherford cross-section. The curves show the CRC calculations for the ^{9}Be + ^{15}N potential scattering (curve <pot>), reorientation of ^{9}Be (curve <reor>), transfer of ^{6}Li-cluster (curve <^{6}Li>) and sequential transfers of protons, neutrons, deuterons, tritons, α-particles (curves <pp>, <nn>, <dd>, <tt>, <$\alpha\alpha$>, respectively) as well as α + d and d + α transfers (curve <αd>). The curves <xy> show the coherent sums of CRC calculations for both transfers $x + y$ and $y + x$. The Σ-curves show the coherent sums of all processes.

As Fig. 5(a) shows, the potential scattering dominates at the small angles and gives contributions over the whole angular range. However, the ^{9}Be ground state spin reorientation dominates at the middle and large angles. The potential scattering is important also at these angles. The transfer reactions give only a small contribution to the ^{9}Be + ^{15}N elastic scattering channel. As the Σ-curves in Figs. 5(a) and 5(b) show, the CRC-calculation with Woods–Saxon potential parameters, listed in Table 3, and the inclusion of the contributions of all possible processes to the elastic scattering channel, describes the ^{9}Be + ^{15}N elastic scattering very well.

In Fig. 6, the ^{9}Be + ^{15}N potential deduced from the ^{9}Be + ^{15}N elastic scattering data is compared with the corresponding double-folding potential. One can see that the real part of the ^{9}Be + ^{15}N potential is in good agreement with the double-folding potential in the peripheral region $3 < r < 7$ fm, where the nuclear interaction dominates over the Coulomb interaction, while the Coulomb interaction is dominant for $r > 7$ fm.

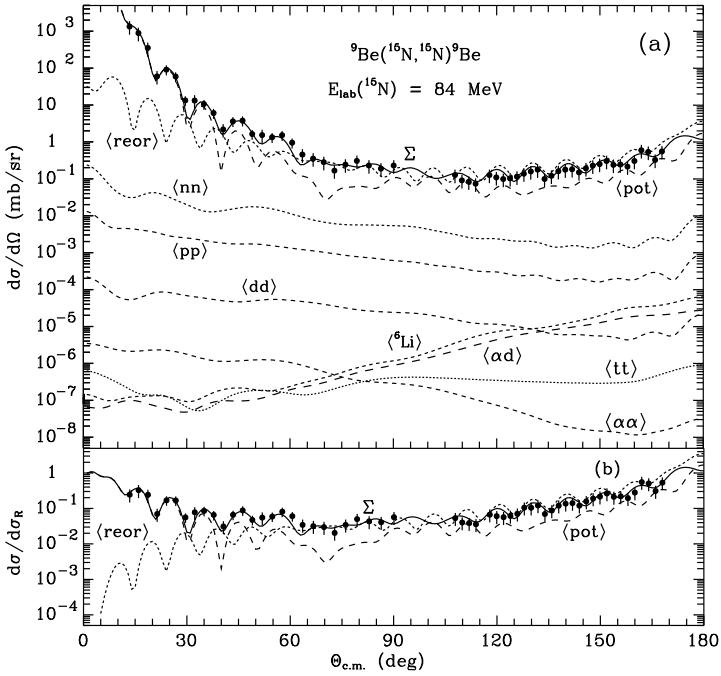

Fig. 5. Angular distributions of the ^{9}Be + ^{15}N elastic scattering (a) in cross-section units and (b) in units of the Rutherford cross-section at the energy $E_{lab}(^{15}N) = 84$ MeV. The dashed curves show the CRC calculations for different nuclear processes (see text). The Σ-curves show the coherent sums of all processes.

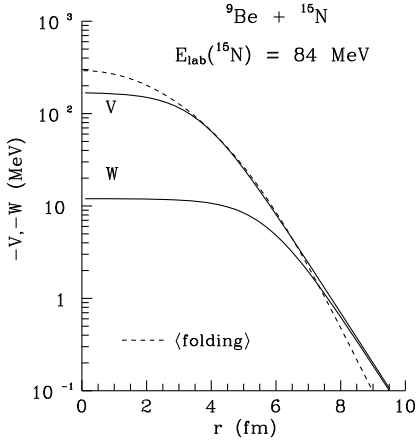

Fig. 6. A comparison of the ^{9}Be + ^{15}N potential with the double-folding potential.

3.3. Inelastic scattering $^9Be + {}^{15}N$

The measured angular distributions of ^{9}Be + ^{15}N inelastic scattering for the transitions to the excited states of ^{9}Be and ^{15}N are given in Figs. 7 and 8. The curves show the CRC-calculations

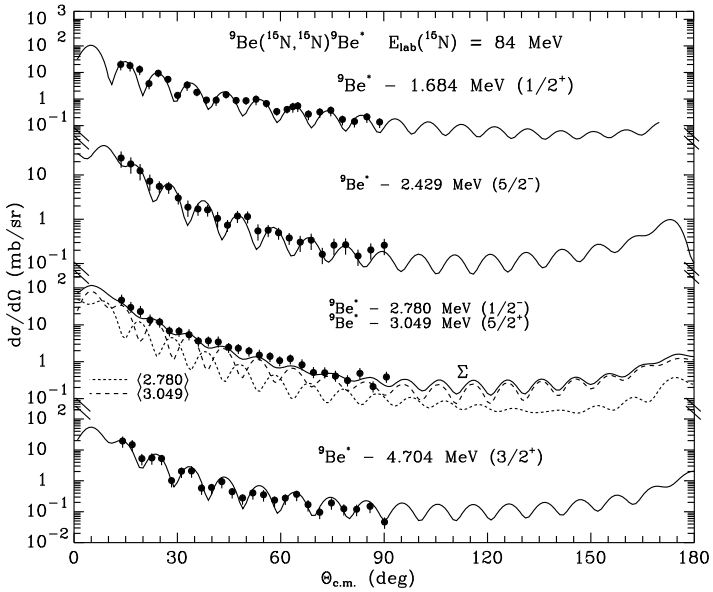

Fig. 7. Angular distributions of the ^{9}Be + ^{15}N inelastic scattering at the energy $E_{\rm lab}(^{15}{\rm N}) = 84$ MeV for the transitions to the excited states of ^{9}Be and ^{15}N. The curves show the CRC calculations. The curve Σ shows the incoherent sum of the CRC calculations for the excited states of ^{9}Be unresolved in the experiment.

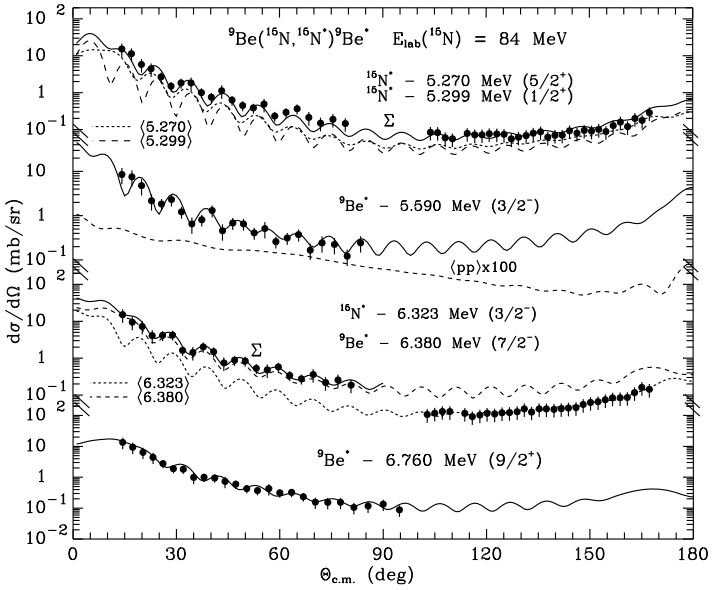

Fig. 8. The same as in Fig. 7 but for other excited states of ^{9}Be and ^{15}N.

for collective (rotational and vibrational) excited states of ^{9}Be and ^{15}N. In Figs. 7 and 8, the dashed curves show the CRC-calculations for individual levels of ^{9}Be and ^{15}N unresolved in the experiment. The curves Σ show their incoherent sums.

In the CRC-calculations of the transitions to the excited states of ^{9}Be and ^{15}N, the form-factor $V_\lambda(r)$ (Eq. (3)) and the ^{9}Be + ^{15}N potential parameters (see Table 3), deduced in the elastic scattering data analysis, were used. As was mentioned previously, the deformation parameters δ_λ of ^{9}Be and ^{15}N were deduced by adjusting them in the CRC calculations to describe the magnitude of the ^{9}Be + ^{15}N scattering data. These parameters are listed in Table 1. The values of some of the δ_λ parameters were found to be the same as those deduced from the analyses of the inelastic scattering data of ^{11}B + ^{15}N [14], ^{9}Be + ^{12}C [19] and ^{9}Be + ^{11}B [20]. These results are important to determine the degree to which the parameter values for these transition strengths can be regarded as reliable. The deformation parameters δ_λ for the 5.59 MeV, 6.38 MeV and 6.76 MeV states of ^{9}Be were deduced here for the first time.

The contributions of transfer reactions (Fig. 5) to the inelastic scattering of ^{9}Be + ^{15}N were also tested. It was found that the sequential proton transfer is the dominant contribution among the possible transfers reactions. In Fig. 8, we show the angular distribution of this reaction for the transition of ^{9}Be to its 5.59 MeV excited state (curve <pp>). One can see that the contribution of this reaction to the $^{9}\mathrm{Be}^{*}_{5.59}$ + ^{15}N inelastic scattering is small. The same situation was observed also for other transitions.

4. Summary and conclusions

New experimental data for the ^{9}Be + ^{15}N elastic and inelastic scattering at the energy $E_{\mathrm{lab}}(^{15}\mathrm{N}) = 84$ MeV ($E_{\mathrm{c.m.}} = 31.5$ MeV) were measured for transitions of ^{9}Be to excited states 1.684–6.760 MeV and ^{15}N to excited states 5.270–6.323 MeV for the first time.

The data were analyzed within the OM and CRC methods. In the CRC analysis, the ^{9}Be + ^{15}N elastic and inelastic scattering, spin reorientation of ^{9}Be as well as one-and two-step transfer reactions were included in the coupled-channels scheme. The low-energy excited states of ^{9}Be and ^{15}N were assumed to have a collective nature (rotation and vibration).

It was found that for the ^{9}Be + ^{15}N elastic scattering, the potential scattering dominates at small angles and gives some contribution to the angular distribution at middle and large angles but the spin reorientation of ^{9}Be dominates in this angular range. One- and two-step transfer reactions give only small contributions to the ^{9}Be + ^{15}N elastic scattering. The deduced ^{9}Be + ^{15}N potential is in good agreement with the calculated double-folding potential in the peripheral interaction region of these nuclei.

The CRC-calculations within the collective model using the deduced deformation parameters δ_λ of ^{9}Be and ^{15}N listed in Table 1, describe very well the data. It was found that the transfer reactions are not important in the ^{9}Be + ^{15}N inelastic scattering.

References

[1] G.R. Satchler, W.G. Love, Phys. Rep. 55 (1979) 183.
[2] G.R. Satchler, Phys. Lett. B 83 (1979) 284.
[3] C.W. Glover, R.I. Cutler, K.W. Kemper, Nucl. Phys. A 341 (1980) 137.
[4] D. Fick, G. Grawert, I.M. Turkiewicz, Phys. Rep. 214 (1992) 1.
[5] S. Ohkubo, Y. Hirabayashi, Phys. Rev. C 89 (2014) 051601(R).
[6] A.A. Ogloblin, et al., Phys. At. Nucl. 66 (2003) 1478.
[7] S. Ohkubo, Y. Hirabayashi, Phys. Rev. C 89 (2014) 061601(R).
[8] S. Ohkubo, et al., Phys. Rev. C 90 (2014) 064617.
[9] S. Ohkubo, Y. Hirabayashi, Phys. Rev. C 92 (2015) 024624.
[10] R.S. Mackintosh, Y. Hirabayashi, S. Ohkubo, Phys. Rev. C 91 (2015) 024616.
[11] J.R.B. Oliveira, et al., J. Phys. G, Nucl. Part. Phys. 40 (2013) 105101.

[12] A.T. Rudchik, et al., Eur. Phys. J. A 44 (2010) 221;
A.T. Rudchik, et al., Eur. Phys. J. A 47 (2011) 50.
[13] A.T. Rudchik, O.V. Herashchenko, K.W. Kemper, K. Rusek, et al., Nucl. Phys. A 941 (2015) 167.
[14] A.T. Rudchik, O.V. Herashchenko, K.W. Kemper, K. Rusek, et al., Nucl. Phys. A 939 (2015) 1.
[15] H.G. Bohlen, W. von Oertzen, R. Kalpakchieva, et al., Nuovo Cimento 111A (1998) 841.
[16] H.G. Bohlen, R. Kalpakchieva, A. Blazevic, et al., Phys. Rev. C 64 (2001) 024312.
[17] H.G. Bohlen, R. Kalpakchieva, W. von Oertzen, et al., Nucl. Phys. A 722 (2003) 3c.
[18] E. Piasecki, M. Antczak, J. Devine, et al., Annual report 2006, Warsaw University, Heavy Ion Laboratory, Warsaw, 2007, pp. 9–39.
[19] A.T. Rudchik, O.A. Momotyuk, V.A. Ziman, et al., Nucl. Phys. A 662 (2000) 44.
[20] A.T. Rudchik, V.M. Kyryanchuk, A. Budzanowski, et al., Nucl. Phys. A 714 (2003) 391.
[21] Yu.F. Smirnov, Yu.M. Tchuvil'sky, Phys. Rev. C 15 (1977) 84.
[22] A.T. Rudchik, Yu.M. Tchuvil'sky, The code DESNA, Kiev Institute for Nuclear Researches report KIYAI-82-12, 1982.
[23] A.T. Rudchik, Yu.M. Tchuvil'sky, Ukr. Fiz. Zh. 30 (1985) 819.
[24] A.N. Boyarkina, Structure of 1p-shell nuclei, Moscow State University report, 1973.
[25] F.C. Barker, Nucl. Phys. 83 (1966) 418.
[26] B.S. Nilsson, SPI-GENOA: an optical model search code, Niels Bohr Institute report, 1976.
[27] I.J. Thompson, Comput. Phys. Rep. 7 (1988) 167.
[28] J. Cook, Comput. Phys. Commun. 25 (1982) 125.
[29] J. Cook, Comput. Phys. Commun. 35 (1984) 775.
[30] H. De Vries, C.W. De Jager, C. De Vries, At. Data Nucl. Data Tables 36 (1987) 495.